fire

MDPI

Article

The Dynamics of Fire Activity in the Brazilian Pantanal: A Log-Gaussian Cox Process-Based Structural Decomposition

Fernanda Valente † and Márcio Laurini *,†

Departament of Economics, FEARP, University of São Paulo, Campus Ribeirão Preto, Ribeirão Preto 14040-905, Brazil; fernanda.valente92@gmail.com

* Correspondence: laurini@fearp.usp.br; Tel.: +55-16-3329-0867

† These authors contributed equally to this work.

Abstract: We present a novel statistical methodology for analyzing shifts in spatio-temporal fire occurrence patterns within the Brazilian Pantanal, utilizing remote sensing data. Our approach employs a Log-Gaussian Cox Process to model the spatiotemporal dynamics of fire occurrence, deconstructing the intensity function into components of trend, seasonality, cycle, covariates, and time-varying spatial effects components. The results indicate a negative correlation between rainfall and fire intensity, with lower precipitation associated with heightened fire intensity. Forest formations exhibit a positive effect on fire intensity, whereas agricultural land use shows no significant impact. Savannas and grasslands, typical fire-dependent ecosystems, demonstrate a positive relationship with fire intensity. Human-induced fires, often used for agricultural purposes, contribute to an increase in both fire frequency and intensity, particularly in grassland areas. Trend analysis reveals fluctuating fire activity over time, with notable peaks in 2018–2021.

Keywords: Brazilian Pantanal; fire modeling; spatiotemporal point process

Citation: Valente, F.; Laurini, M. The Dynamics of Fire Activity in the Brazilian Pantanal: A Log-Gaussian Cox Process-Based Structural Decomposition. *Fire* **2024**, *7*, 170. https://doi.org/10.3390/fire7050170

Academic Editors: João Neves Silva and Duarte Oom

Received: 26 March 2024
Revised: 16 May 2024
Accepted: 16 May 2024
Published: 19 May 2024

1. Introduction

The Pantanal biome is recognized as the world's largest wetland ecosystem, situated in the Upper Paraguay River Basin (UPRB) in South America, between the Cerrado and Amazon biomes [1]. The Brazilian Pantanal is situated in the southwest region, mostly in the state of Mato Grosso do Sul (65%), but also in the state of Mato Grosso (35%) [2]. The biome is marked by the well-defined dry and wet seasons, which cause periodic fluctuations in the water level (flood pulse), shaping the scope of terrestrial and aquatic places on the lowland, and influencing the fauna and flora. The vegetation in the Pantanal is heterogeneous, with several vegetation classes identified, also serving as the habitat for substantial populations of animals, including threatened species [3].

The high biological diversity of the Pantanal has attracted considerable attention, rendering this biome increasingly susceptible to anthropogenic threats. Over the past few decades, the Pantanal has experienced a rapid evolution of its agricultural and livestock systems, with natural vegetation areas being replaced by production zones [4–6]. The monitoring activities of 2012–2014 to assess the environmental impact in the UPRB have identified that 58% of the original vegetation in the plateau areas was converted to anthropic uses, whereas in the lowlands this conversion corresponds to 42%. In addition, the report also has found that 99% of all converted areas have been used as pastureland, 0.6% for agriculture, and 0.4% for mining and urban areas [7].

Related to agriculture and cattle ranching, the inclusion of exotic grass species and the burning practice are important threats in the region. As a consequence of replacing the original vegetation by cultivated pastures and uncontrolled fires, severe erosion has led to changes in the hydrological regimes and the patterns of water flow [4]. As discussed by [8], changes in the vegetation productivity in these landscapes are likely linked to changes in

rainfall and the flood pulse, with different responses based on position relative to inundated areas. As a consequence, these changes in the vegetation cycle can lead to changes in the fire activity. Although occasional fire plays an important ecological role in wetland, with positive impacts on some vegetation structure and nutrient recycling [9,10], fire is one of the most important environmental disturbances, affecting the variations in flood and dry periods, and, as a consequence, changing the required time of plants and animals to recover after the dry periods [11].

In recent years, extensive and more frequent fire events have been reported in the Brazilian Pantanal. For instance, in 2020, more than 22 thousand fire outbreaks were registered in the Pantanal, with a burned area of 33,000 km², exceeding by 176% the historical record of fire outbreaks registered in 2005 since the beginning of the monitoring by the *Instituto Nacional de Pesquisas Espaciais* (INPE) in 1998. In addition, the area burnt in 2019 in the Brazilian Pantanal was surprisingly 996% higher than in 2018, which is particularly high when compared with the neighboring biomes (Cerrado and Amazon) that have recorded an increase around 40% and 65% of the burned area from 2018 to 2019, respectively. In addition, it is worth noting that 95.72% of the fire events in the Pantanal have occurred in native vegetation, whereas only 4.28% was in anthropized areas.

One reason for this increase may be related to land use and climate changes, which have the potential to affect the rainfall intensity and the dry period, thus favoring the frequency of fire events, mostly human-induced (accidentally or deliberately), which tends to start in grasslands and then move to woodlands [10]. In the absence of specific legislation requiring that landowners restrict a minimum percentage of native vegetation cover in the farms, an average vegetation loss of around 10% for the plateau and 3% for the lowland is expected by 2050 [12,13]. Given the widely expected trend of agriculture and livestock expansion, and the importance of the Brazilian Pantanal to provide ecosystem services and the economic valuation of the region [1,14–16], there is an urgency to evaluate the possible changes in the patterns of fire occurrence in the region, in order to find solutions to minimize the impacts.

In this sense, to monitor the patterns of fire occurrence in the Brazilian Pantanal, we propose to model the dynamics of the point process of geolocated events (fire spots) based on remote sensing data resources through a spatiotemporal decomposition for the spatiotemporal point process, for the period 1999–2022. In particular, we use a novel dynamic representation of a Log-Gaussian Cox Process (LGCP), where the intensity function is modeled through decomposition of components in trend, seasonality, cycles, covariates, and spatial effects [17–20], assuming that spatial effects are time varying, based on an autoregressive functional structure.

Our method introduces a dynamic modeling approach that incorporates spatiotemporal decomposition to capture the underlying dynamics of fire events. This method utilizes remote sensing data to model the point process of geolocated events (fire spots), allowing for a comprehensive understanding of fire patterns over time and space. By employing techniques such as the Log-Gaussian Cox Process (LGCP), which builds upon the Bayesian framework for Log-Gaussian Cox Processes originally advanced by [21], and incorporating common latent components and time-varying spatial effects, this approach accounts for the evolving nature of fire dynamics in the region.

Integrating remote sensing technology with statistical modeling, the methodology offers a robust framework for assessing and predicting fire occurrences in the Pantanal, contributing to the advancement of environmental science research. Consequently, it provides a robust means for investigating potential anthropogenic factors contributing to the spatiotemporal distribution of fires. This modeling approach provides a robust foundation for understanding and analyzing the spatiotemporal dynamics of fire occurrences in the Pantanal.

This article has the following structure. Section 2 presents a brief literature review on fire occurrence patterns in the Pantanal and the methods used in the analysis. The analyzed data are presented in Section 3, and the methodology used in this study is placed in

Section 4. The results are presented and discussed in Section 5, and the general conclusions are in Section 6. The Appendix contains additional discussions of the representation used for the LGCP (Appendix A.1) and the spatial covariance function (Appendix A.2) and additional results using a non-separable version of the model (Appendix A.3).

2. Literature Review

2.1. Literature Review on Fire Activity in the Brazilian Pantanal

Despite the existence of long-term studies evaluating variations in rainfall patterns in the Pantanal and their consequences for fire frequency, research on climate landscape dynamics remains underdeveloped in the region [22]. Specifically, regarding fire occurrences, there exists a notable research gap that our study intends to address. Moreover, the advancement of remote sensing technology has emerged as a tool for assessing fire events and monitoring potential shifts in their patterns.

The significant surge in fire outbreaks witnessed in the Pantanal during 2020 [23] has sparked crucial discussions regarding both climatic and anthropogenic factors influencing this unprecedented occurrence. Ref. [24] thoroughly analyzes the convergence of climatic and environmental conditions contributing to this phenomenon. Their study identifies a severe drought, extreme temperatures, and increased fuel availability as key elements underpinning the record number of fires in 2020. For a broader examination of this correlation within Brazil, a comprehensive discussion is available in [25]. Additionally, ref. [26] addresses the impact of heatwaves, projecting their likelihood of recurrence in the future of the Pantanal.

However, it is noteworthy that not all climatic influences are equally pertinent in explaining the fire patterns observed in the Pantanal. Ref. [27] investigates the role of lightning as fire igniters, revealing limited evidence of their association with fires, thereby suggesting that human-related activities primarily drive ignitions.

Anthropogenic aspects, including changes in land use (e.g., [28,29]), and the implications of climate change, are discussed in [30]. This study analyzes how the combined effects of precipitation, temperature, soil moisture, and evapotranspiration exhibited atypical behavior during this period. Furthermore, changes in land use, particularly land use and land cover (LULC) classes, are underscored as significant contributors to the 2020 fire patterns by [31]. Their findings demonstrate a preference for forest regions in the 2020 fires, with forests and grasslands experiencing larger fire patches compared to crops, consistent with results from [32]. This study highlights the pivotal role of reduced water surface area in the Pantanal and emphasizes that 84% of new fires occurred within natural vegetation, with 39% affecting forests—an alarming 514% increase. Forest fires alone accounted for 47% of the carbon loss in 2020. Notably, a staggering 70% of the fires in 2020 transpired within rural properties, with 5% in indigenous lands and 10% in protected areas, accentuating the complex interplay between human activities and environmental factors in shaping fire dynamics in the Pantanal.

2.2. Literature Review on the Method

Our objective is to analyze the temporal and spatial patterns of the occurrence of fires in the Pantanal biome, using the structure of spatial points processes [33,34]. Spatial point processes are a mathematical framework used to model the spatial distribution of points or events occurring in a particular region of interest. The basic idea behind spatial point processes is to describe the random occurrence of points within a defined spatial domain. These processes can be either discrete or continuous, depending on the nature of the underlying phenomena. In a discrete spatial point process, the points are distinct and separate entities, whereas in a continuous spatial point process, points are distributed continuously over space, which is the form used in our analysis.

There are various types of spatial point processes, each with its own characteristics and properties [34]. Some common types include the homogeneous Poisson Process, that is the simplest type of spatial point process, where points are distributed randomly

and independently throughout the spatial domain, with a constant intensity rate. In the inhomogeneous Poisson process, the intensity rate varies spatially, meaning that the probability of finding points at different locations in the spatial domain is not uniform.

The Log-Gaussian Cox Process (LGCP) [34–36] is a spatial point process that combines elements of Gaussian processes with Cox processes to model spatial point patterns where the intensity varies smoothly over space. Applications of LGCP in health data modeling, epidemiology, and species distribution can be found at [37–39], and in the modeling of fire occurrence in [19,20,40]. This model is particularly useful when the intensity of point occurrences is believed to be influenced by underlying continuous spatial covariates. In LGCP, the log of the intensity function, $\log(\lambda(s))$, is modeled as a Gaussian process.

A Gaussian process [41] is a collection of random variables, any finite number of which have a joint Gaussian distribution. It is fully specified by its mean function and covariance function. LGCP allows for the inclusion of spatial covariates, such as temperature or land use, which are believed to influence the intensity of point occurrences. These covariates can be incorporated into the mean function of the Gaussian process to capture their effect on the intensity.

The inference procedures for the LGCP are based on the estimation of intensity function. This involves estimating the spatial variation in the intensity of point occurrences. Using the estimated intensity function we can realize the spatial prediction, predicting the expected number of points within the spatial domain [34].

To properly deal with point pattern data we use a spatiotemporal decomposition based on a LGCP, where the log-intensity function is given by a Gaussian Markov random field (GMRF) ([41]). This framework is a flexible way to overcome the limited structure of the Poisson process, by allowing to introduce more complex stochastic structures in the intensity function, controlling for general processes of spatial dependence.

However, inference procedures on the LGCP are difficult given the fact that the likelihood of these processes is analytically intractable. To bypass this problem, Ref. [21] proposed to approximate the LGCP likelihood through the stochastic partial differential Equation (SPDE) approach [42] representation of the latent random field, which is a computationally effective way to deal with spatiotemporal models in the context of point pattern data.

In addition, as proposed by [18,43], the LCGP structure allows us to estimate long-term changes and transient components through a structural decomposition (à la [44]) of the intensity function. We present the details of the methodology used in the analysis in Section 4.

3. Data

Our main goal is to analyze the changes in the permanent and transitory patterns of fire occurrence in the Brazilian Pantanal biome, which was delimited based on The Map of Biomes and Coastal-Marine System of Brazil from *Instituto Brasileiro de Geografia e Estatística* (IBGE) Available at https://www.ibge.gov.br/geociencias/cartas-e-mapas/informacoes-ambientais/15842-biomas.html, accessed on 31 January 2023. For that, we use daily data of fire spots in the Brazilian Pantanal from July 1998 to December 2022, provided by the Programa Queimadas Data and more information available at http://queimadas.dgi.inpe.br/queimadas/portal, accessed on 31 January 2023, from Brazilian National Institute of Spatial Research (*Instituto Nacional de Pesquisa Espacial*-INPE). We also included covariates that could be important in the fire observations since our data set includes fire occurrences of different causes, such as human sources and natural causes, which can be influenced by climate variables. In particular, we included information on maximum temperature, rainfall, and land use/land cover from 1998 to 2022, as explained below.

The daily data of fire spots used in the paper are provided by the Programa Queimadas (data and other information available at https://terrabrasilis.dpi.inpe.br/queimadas/bdqueimadas/), accessed on 31 January 2023, from the Brazilian National Institute of Spatial Research (*Instituto Nacional de Pesquisa Espacial*-INPE), which uses two different sensors as

the main source of information, namely Moderate Resolution Imaging Spectroradiometer (MODIS) Aqua and Terra products, and the Advanced Very High Resolution Radiometer (AVHRR) from the National Oceanic and Atmospheric Administration (NOAA).

Initially, from 1 June 1998 to 3 July 2002, NOAA-12 (with the AVHRR sensor, passing in the late afternoon) was employed. Subsequently, AQUA_M-T (with the MODIS sensor, passing in the early afternoon) took over. This transition led to a disruption in the number of observed outbreaks in our data analysis, potentially underestimating the true count of burning spots and forest fires. Despite this, employing the same detection methodology and generating images at similar times across the years allows us to utilize results from the "reference satellite" to scrutinize spatial and temporal trends in outbreaks.

Note that the fire point data released by INPE coincides with the dataset from NASA and the University of Maryland (UMD) in the USA, referred to as "Collection 6", which has been in operation since 2016, supplanting "Collection 5" globally. INPE did the same with its MODIS database (AQUA and TERRA) in March/2017. This comprehensive replacement of the database necessitated reprocessing thousands of past images, driven by advancements in image focal point extraction algorithms, yielding more dependable end products. Prior to "Collection 5", INPE maintained its own detection algorithm for MODIS images, ensuring robust data. However, with the advent of "Collection 6", this approach became redundant, prompting the Queimadas Program to adopt the same algorithm as NASA and UMD for detecting MODIS outbreaks. This alignment renders the databases compatible, thereby broadening the range of potential applications for the data. See the notes at https://terrabrasilis.dpi.inpe.br/queimadas/portal/faq/index.html, accessed on 31 April 2024, on the properties and limitations of the database.

However, despite the discontinuity in the observed data, it is worth noting that even indicating a fraction of the actual number of fires and forest fires, using the same detection method and collecting images at close times over the years, the results obtained from both reference satellite allow us to analyze the spatial and temporal trends of the fires. In this sense, to reach our goal, we use the data from the MODIS/NASA and AVHRR/NOAA satellites, with the data validation carried out by the Queimadas system. The dataset provides geographical information and the time and period of fire spots within the Brazilian Pantanal, which is located within the states of Mato Grosso do Sul and Mato Grosso in the southwest region. In addition, in order to provide a clearer interpretation of the results obtained, we used a quarterly aggregation of the daily data, which is the sum of the observed fire events in each quarter of the year.

We plotted the number of quarterly observed fire spots (see Figure 1), from 1998 to 2022, where it is possible to see the unprecedented fire outbreak in 2020. To emphasize the large number of fire outbreaks detected in 2020, in Figure 2 we show the observed fire events (black dots) in the Brazilian Pantanal in the third quarters of 2018 and 2020 (on the top of the figure). Furthermore, in the bottom of Figure 2, it is possible to observe the non-parametric kernel density estimate of the intensity function [34] of the occurrence process. We choose to compare the fire outbreak in 2020 with 2018 since the latter presented fire patterns close to the average in comparison to the past 20 years. Based on Figure 2, we can see a notable increase in the intensity and spatial distribution of fire outbreaks in 2020 compared to 2018.

Regarding the covariates, it is worth discussing a meaningful limitation related to the selected covariates in our analysis. Since the proposed model performs a spatiotemporal analysis for the occurrences of a process observed continuously in space, the covariates must be available at every location of the interest region within the observation window. Due to this methodological constraint, the number of available covariates is limited, and we were able to include limited information in climatic patterns and land use. In particular, regarding the rainfall and maximum temperature data, we calculated the spatially continuous projections from weather station data, following the [43] methodology, as discussed below.

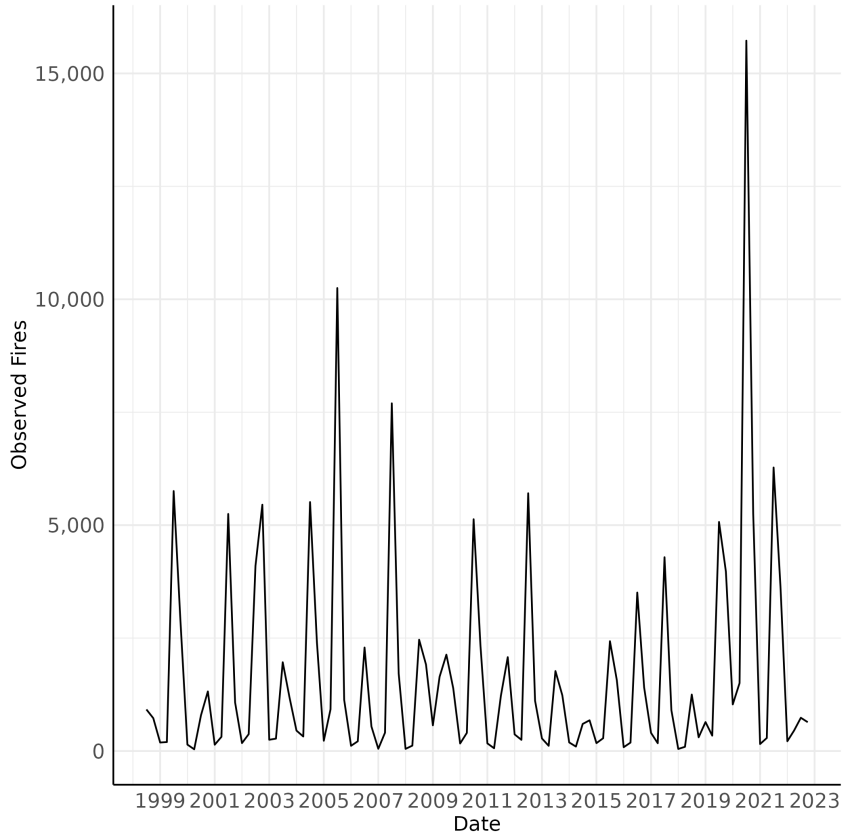

Figure 1. Observed fire events by quarter in Brazilian Pantanal.

The rainfall data were constructed using the time series of the monitoring stations provided by the Brazilian National Agency of Waters (*Agência Nacional de Águas*—ANA) and National Institute of Meteorology (*Instituto Nacional de Metereologia*—INMET), whereas the maximum temperature data were obtained based on the information provided by the INMET. For both data, we calculated the spatially continuous projections for each period in the sample, following the methodology proposed by [43].

By adopting this methodology, we were able to avoid some common problems faced in the analysis of the data sources used in climatology; namely, the dimensionality of the spatiotemporal dataset, the importance of the spatial features, and missing data. In particular, by combining a structure of trend-cycle decomposition with the continuous spatial formulation, the approach allows us not only to estimate the patterns throughout the spatial continuum and how it propagates throughout the area of interest, but also provides a way to solve the missing data problems by adding the latent components with the prediction obtained for the spatial effect in the geographic position of the weather station using the continuous projection of the spatial effect, without the necessity of additional treatments for missing data or interpolation methods. In summary, this methodology allows us to control possible changes in weather patterns, and is also based on possible changes in trends, seasonality, and cycles in climate data.

In addition, we included, as categorical variables, yearly information on land use/Land Cover (LULC) provided by the Landsat-based MapBiomas project (Collection 5). The database includes annual historical maps of each biome, which contains a hierarchical system of classification of land use/land cover following the Food and Agriculture Organization (FAO) and *Instituto Brasileiro de Geografia e Estatística* (IBGE) classification systems. The first level contains six classes; namely, forest, non-forest formation, farming, non-vegetated area, water, and non-observed. Forest constitutes natural forest and forest plantation, whereas the non-forest natural formation includes wetland, grassland, salt flat, rocky outcrop, and other non-forest formations. The farming class includes pasture,

agricultural land, and mosaic. The non-vegetated areas are defined by beaches and dunes, urban areas, mining, and other non-vegetated areas. Finally, the water class includes rivers, lakes, oceans, and aquaculture. The accuracy statistics vary according to the level and biome. In particular, considering the Pantanal biome, the first level has 81.6% overall accuracy with 12.9% allocation mismatch and 5.6% quantity mismatch. For the second and third levels, the overall accuracy is 73.5%, whereas the allocation and quantity mismatch are 17.5% and 9%, respectively. The methodology overview of the MapBiomas project is available at https://mapbiomas.org/, accessed on 31 January 2023, whereas the accuracy assessment for the Brazilian biomes is available in the MapBiomas accuracy statistics web page https://mapbiomas.org/en/estatistica-de-acuracia?cama_set_language=en, accessed on 31 January 2023. A detailed description of the MapBiomas land use/land cover classification can be found in Table 1, whereas Figure 3 shows a map with the Mapbiomas classifications for the year 2019.

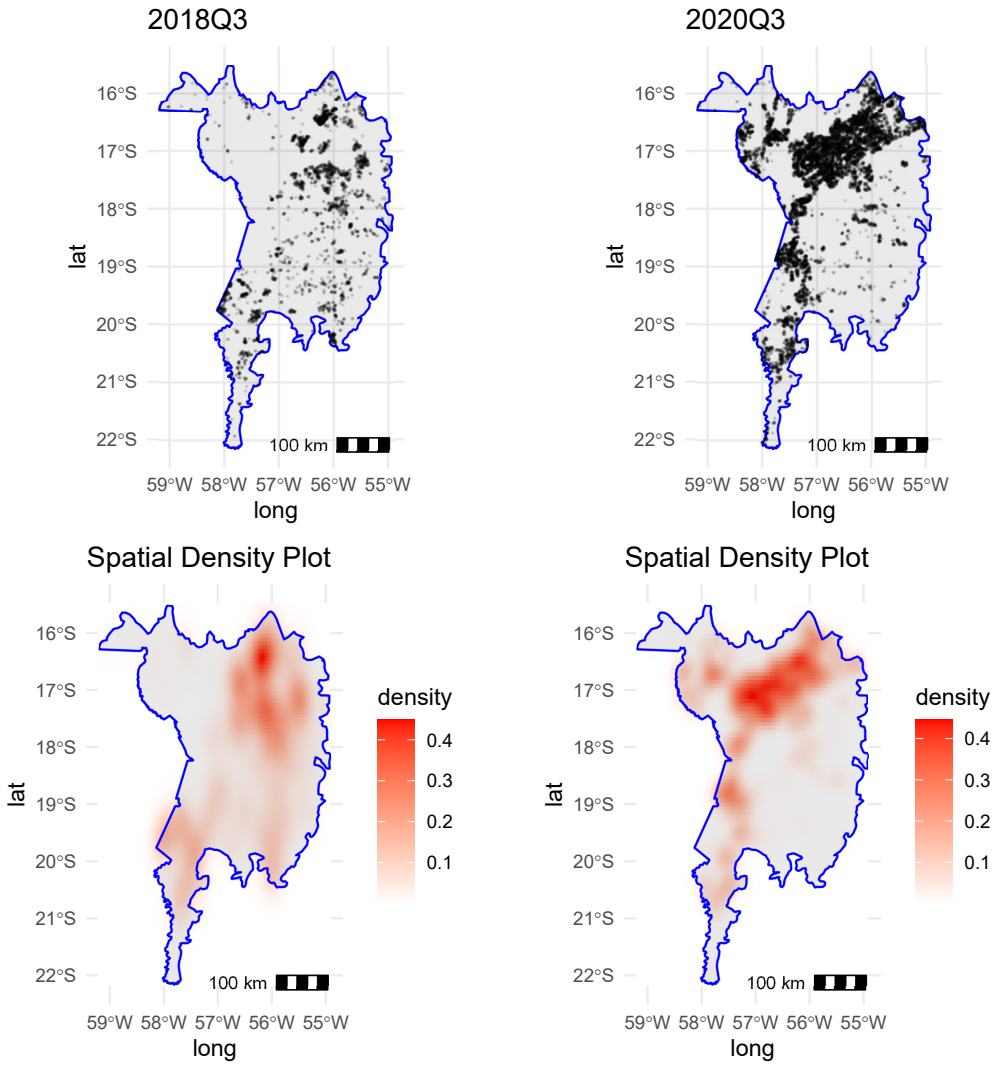

Figure 2. Observed fires (top left and top right) and non-parametric intensity estimation (bottom left and bottom right)—2018Q3 (top and bottom left) and 2020Q3 (top and bottom right).

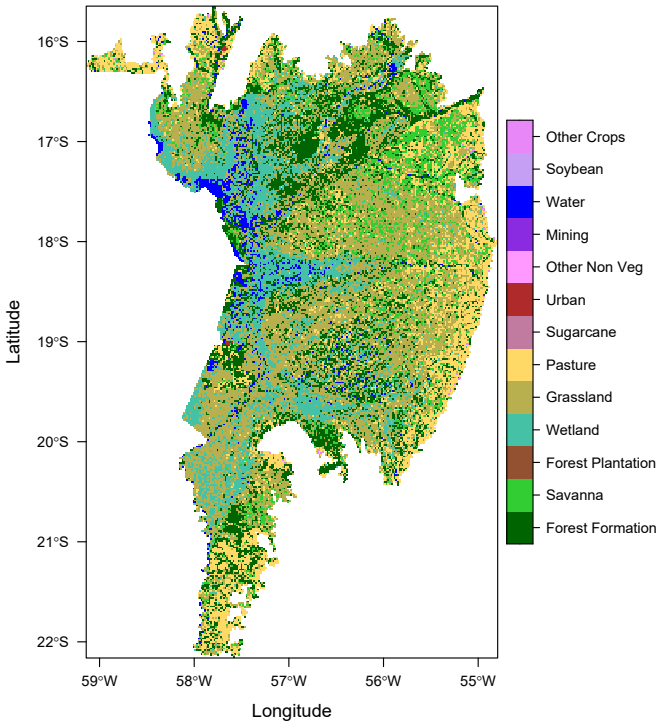

Figure 3. Land use/land cover in the Brazilian Pantanal from MapBiomas—2019.

Table 1. MapBiomas land use/land cover classification.

LULC	ID
1. Forest	1
1.1. Natural Forest	2
1.1.1. Forest Formation	3
1.1.2. Savanna Formation	4
1.1.3. Mangrove	5
1.2. Forest Plantation	9
2. Non-Forest Natural Formation	10
2.1. Wetland	11
2.2. Grassland Formation	12
2.3. Salt Flat	32
2.4. Rocky Outcrop	29
2.5. Other Non-Forest Formation	13
3. Farming	14
3.1. Pasture	15
3.2. Agriculture	18
3.2.1. Temporary Crop	19
3.2.1.1. Soybean	39
3.2.1.2. Sugar cane	20
3.2.1.3. Other Temporary Crops	41
3.2.2. Perennial Crop	36
3.3. Mosaic of Agriculture and Pasture	21
4. Non-Vegetated area	22
4.1. Beach and Dune	23
4.2. Urban Infrastructure	24
4.3. Mining	30
4.4. Other Non-Vegetated Areas	25
5. Water	26
5.1. River, Lake, and Ocean	33
5.2. Aquaculture	31
6. Non-Observed	27

4. Methods

Our aim is to examine the temporal and spatial distribution of fires within the Pantanal biome, employing spatial point processes to analyze the patterns. In particular, we proposed to decompose the intensity function into latent factors of trend, seasonality, and cycle, along with covariates and spatial effects.

In the analysis of the temporal pattern, the main object is the trend component, which shows the evolution of the average level of occurrences over time, and thus shows the persistent patterns of fire occurrence in the Pantanal. Variations in this component may indicate variations that are possibly related to changes in the patterns of land-use management in agricultural activities, such as the use of burning for the removal of native vegetation and later use in pastures and plantations. This interpretation is possible by controlling the climatic effects through covariates, and also by controlling other possible non-permanent effects by including the seasonality and cycle components. In addition to the inclusion of these common temporal and covariate components, the model used in the analysis includes a structure of time-varying spatial random effects, which allow the capture of the remaining spatial patterns, also allowing us to analyze if there are other effects in the fire patterns that have spatial dependence.

To provide a clearer idea of the method employed to reach our goals, we present a brief description of the likelihood approximation proposed by [21]. Our approach is based on the extension of the static approach to Log-Gaussian Cox Processes proposed in [21] for a spatiotemporal dynamic structure, modeling the pattern of fire occurrences over time. Herein, we provide some details about the model structure used in our analysis. Assuming a bounded region $\Omega \subset \mathbb{R}^2$, the number of points within a region $D \subset \Omega$ in period t is Poisson distributed with mean $\Lambda_t(D) = \int_D \lambda(s,t)\, ds$, where $\lambda(s,t)$ is the intensity surface function of the point process. Under this structure, the likelihood of the Poisson process Y_t is given by

$$\pi(Y_t \mid \lambda) = \exp\left\{ |\Omega| - \int_\Omega \lambda(s,t)\, dsdt \right\} \prod_{s_i \in Y_t} \lambda(s_i, t). \tag{1}$$

We assume the structure of a spatiotemporal Log-Gaussian Cox Process, decomposing the spatiotemporal log-intensity function $\log \lambda(s,t)$ as a latent random field given by the sum of covariates and latent stochastic components:

$$\begin{aligned} \log \lambda(s,t) &= \mu_t + s_t + c_t + z(s,t)\beta + \xi(s,t) \\ \mu_t &= \mu_{t-1} + \eta_\mu \\ s_t &= s_{t-1} + s_{t-2} + \ldots + s_{t-m} + \eta_s \\ c_t &= \theta_1 c_{t-1} + \theta_2 c_{t-2} + \eta_c \\ \xi(s,t) &= \Theta \xi(s, t-1) + \omega(s,t) \end{aligned} \tag{2}$$

where μ_t is the long term trend, s_t represents the seasonal components, c_t is a cycle component represented by a second-order autoregressive process with complex roots, $z(s,t)$ is a set of covariates observed in the location s and period t, and $\xi(s,t)$ are the spatial random effects represented by the Gaussian process $\omega(s,t)$ continuously projected in space and given by

$$Cov[\omega(s,t), \omega(s',t')] = \begin{cases} 0 & \text{if } t \neq t' \\ \sigma^2 C(h) & \text{if } t = t' \end{cases} \qquad \text{for } s \neq s' \tag{3}$$

In this structure, the trend component is modeled as a first-order random walk, which is a way widely used to model persistent components in time series models. The seasonality component is given by components that add up to zero within the year, which incorporate seasonal deviations from the series average in each period. The cyclic component is modeled with a second-order stationary autoregressive process, which is a parsimonious way of recovering periodic patterns in time series.

The spatial component is defined by a spatially continuous covariance function. By assumption, $C(h)$ is a covariance function of the Matérn class, which can be written as

$$C(h) = \frac{2^{1-\nu}}{\Gamma(\nu)}(\kappa||h||)^{\nu}K_{\nu}(\kappa||h||) \tag{4}$$

where $h = ||s - s'||$ is the Euclidean distance between locations s and s', $\kappa > 0$ is a spatial scale parameter, $\nu > 0$ is the smoothness parameter, and K_{ν} is a modified Bessel function.

The spatial random effects included in the model are a statistical mechanism to capture the aggregate effect of all variables omitted in the model that present a structure of spatial dependence, and the addition of this component serves to capture the spatial heterogeneity generated by the variables omitted from the model. Its addition is especially relevant in models where the space is treated continuously as such models require covariates that are also continuously observed in space, and due to measurement difficulties and costs, the observed set of covariates is quite limited. Therefore, the spatial random effects component allows controlling the compound effect of omitted covariates in space and time, allowing robust estimation of the parameters associated with the covariates and latent factors included in the model.

To sum up, our goal is to obtain the intensity function of a latent spatiotemporal points process model, which is decomposed into components of trend, seasonality, cycle, plus the effect of covariates and the so-called spatial random effect, which captures the local effects not captured by the other components. By using this structure, we are able to assess possible changes in the patterns of fire occurrence in the Brazilian Pantanal. In addition, the reason to incorporate covariates in the analysis is to control the impact of climate variables and other effects related to land use and land cover.

As discussed before, we extend the likelihood approximation proposed by [21] to represent the likelihood function of a spatiotemporal LGCP and perform inference for hyperparameters and latent components using a Bayesian method by means of Integrated Nested Laplace Approximations introduced in [45] using the SPDE representation for the latent log-intensity function proposed by [42] and the approximation of the likelihood function introduced by [21]. We present the main details of these likelihood approximations for the LGCP in Appendix A.1 and the SPDE representation in the Appendix A.2.

A relevant concern about the formulation given by Equation (2) is the identification of the model, composed of the sum of several latent components. A formal analysis of the identification of this model would require analyzing the spectral representation of the LGCP process with the log-intensity function used in our analysis, since the identification of the latent components of trend, cycle, and seasonality in state space representations is based on the spectral generating function, as discussed by [46]. As we are using a direct representation in the time and space domains for this process, we do not have a spectral representation available, and thus the identification is based on the numerical optimization properties of the inference procedures.

Since we are using Bayesian inference methods through Integrated Nested Laplace Approximations, it is possible to verify signs of identification problems through the numerical procedures for estimating the posterior mode necessary for the application of Laplace approximations. Signals of identification problems can be noted through the presence of singularities and negative eigenvalues in the numerical Hessian matrix evaluations used in the optimization procedure used for mode finding.

In estimating all the models used in this work, there were no signs of numerical problems related to non-identification conditions, which shows that empirically the model seems to be identified. We assumed additional restrictions on the definition of random effects, assuming that the cycle (AR(2)), seasonality, and the spatial random effect sum to zero in time, avoiding problems of identification with the process average. It is also important to note that the estimates are robust to the initial values used in the numerical optimization, indicating the absence of multiple modes, which would also be evidence of a

lack of identification. Thus, although we do not have a formal proof of identification in our model, the evidence of numerical stability is favorable to the parameterization used.

5. Results and Discussion

In this section, we discuss the results of the final specification for the analyzed model based on Equation 2, where the statistically significant covariates were rainfall, given by the rainfall accumulated in the quarter, and land use/cover variables in each location analyzed. Regarding the maximum temperature variable, it did not provide a statistically significant pattern to explain the variation in the fire events, even though there was a long-term increase in maximum temperature trends in the Pantanal region.

As discussed in the Data and Methods sections, the estimation of the spatiotemporal model is based on the construction of a mesh, which represents a discretization of the continuous space for the evaluation of the likelihood function of the Log-Gaussian Cox Process using the SPDE approximation to numerically evaluate the latent random field. In this work, we use a mesh with 1002 triangles, as shown in Figure 4. Through the INLA method, we estimated the posterior distribution of the parameters described in Equation (2).

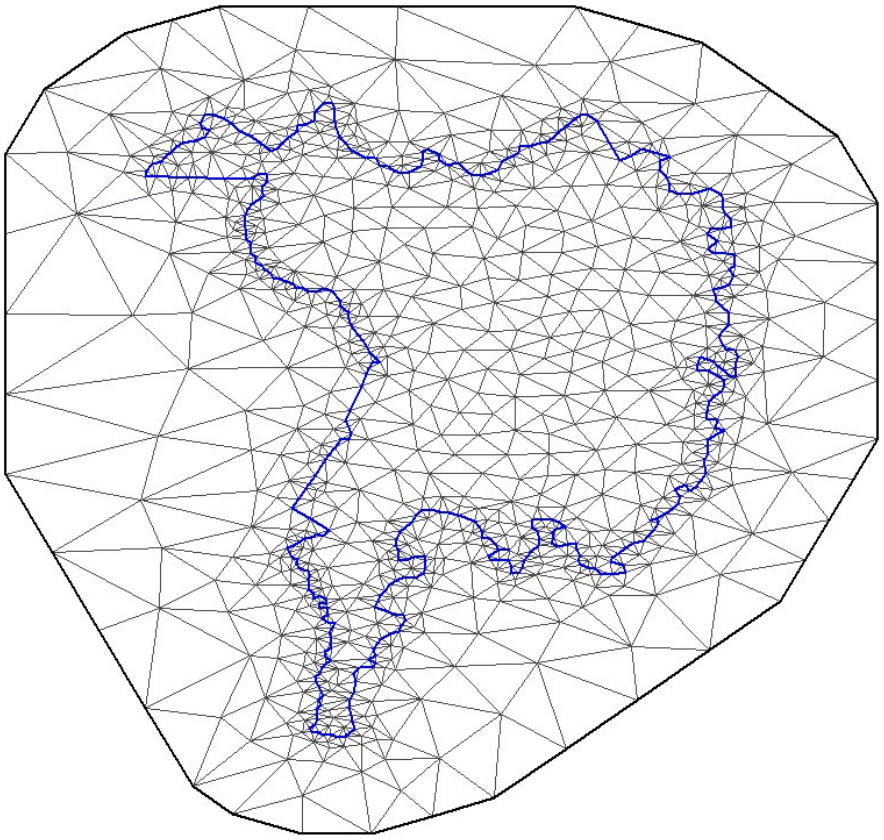

Figure 4. Spatial mesh of the Brazilian Pantanal.

The estimated parameters of Equation (2) are the precision of the trend component ($1/\eta_\mu$), seasonal component ($1/\eta_s$), and cycle component ($1/\eta_c$), the parameters of the second-order autoregressive process of the cycle component (PACF1 and PACF2), the parameters associated with the set of observed covariates (β), the parameters of spatial covariance ($\log\tau$ and $\log\kappa$), and the parameter of spatial time dependence (Φ) are available in Table 2. We comment below on the effect of the covariates in the model, and then on the estimated parameters and latent components.

Table 2. Estimated parameters.

	Mean	SD	0.025 Quant	0.5 Quant	0.975 Quant	Mode
Fixed effects						
Rainfall	−0.001	0.000	−0.002	−0.001	−0.001	−0.001
Forest formation	0.071	0.036	0.000	0.071	0.141	0.071
Savanna formation	0.084	0.038	0.009	0.084	0.158	0.084
Grassland formation	0.185	0.036	0.115	0.185	0.255	0.185
Random effects						
Precision for trend	5.468	0.159	5.175	5.468	5.820	5.426
Precision for seasonality	13,100.823	324.050	12,436.171	13,096.492	13,783.429	13,095.810
Precision for cycle	1.220	0.033	1.149	1.219	1.284	1.227
PACF1 for cycle	0.069	0.012	0.044	0.069	0.093	0.069
PACF2 for cycle	−0.128	0.012	−0.154	−0.128	−0.105	−0.125
Log τ	−4.153	0.008	−4.171	−4.154	−4.137	−4.152
Log κ	2.168	0.007	2.153	2.168	2.183	2.168
Group Φ	0.345	0.004	0.337	0.345	0.355	0.345

Note: The fixed effects denote the parameters for the covariates in the model. Precision denotes the estimated precision (inverse of variance) for the latent component. PACF1 and PACF2 denote the first- and secord-order partial autocorrelations of the cycle component. Log τ and Log τ are the parameters of the Matérn covariance function, and Group Φ denotes the autoregressive persistence of Matérn covariance.

From the obtained results (see Table 2), it is possible to observe a negative relation between rainfall and the intensity of fire events, i.e., the lower precipitation leads to higher fire intensity. Our findings align with those presented in [24], which pinpoint severe drought and heightened fuel availability as pivotal factors driving the unprecedented surge in fires during 2020, corroborating the conclusions discussed by [25].

On the other hand, natural forests such as forest formation, savanna, and natural grassland have a positive effect on fire intensity. It is important to emphasize that other types of land use/cover were not statistically significant in terms of the intensity of the process, especially land use in agricultural activities. It is not surprising that ecosystems formed by savannas and grasslands are positively related to fire intensity since they are mostly fire-dependent ecosystems [47].

Our results are consistent with the patterns found by [31,32]. Their findings demonstrate a preference for forest regions in the 2020 fires, with forests and grasslands experiencing larger fire patches compared to crops. Ref. [31] highlights the finding that 84% of new fires occurred within natural vegetation, with 39% affecting forests. The estimated parameters for the forest, savanna, and grassland vegetation formations indicate different magnitudes of impact on the intensity of fires, with a greater intensity of occurrence in savanna and especially grassland covers, with posterior mean parameters of 0.084 and 0.185, respectively, compared to the value of 0.071 for forest formations. This implies a greater susceptibility of these formations to the occurrence of fires.

Indeed, fires in this type of formation are typically mild and frequent, often occurring in the transitional months between seasons and providing benefits to the fauna and flora [48,49]. However, in this kind of vegetation, there is also the occurrence of anthropogenic fires, which are used to clean the field, control pests, and stimulate the regrowth of grasses for cattle, increasing the fire frequency.

Natural fires are usually controlled by the rainy season, whereas human-induced fires also usually occur in the dry season and are more intense than natural fires, spreading more easily and without rain to extinguish them. As a consequence, recurrent human-induced fires can affect the spatial pattern and intensity of the fire activity even in fire-dependent environments. In combination with drought, these alterations can cause severe and catastrophic fires, as those recorded in 2020 in the Pantanal [49]. Additionally, it is important to emphasize that riparian and gallery forests along water bodies in the grassland and savanna formation are classified as fire-sensitive environments, and can be gradually reduced when in contact with recurrent fires [10].

However, it is important to highlight that our data sources do not distinguish whether the fire occurrence is natural or caused by human actions, and thus additional studies are needed to better elucidate the role of human influences in fire activity of this kind of vegetation.

On the other hand, forest formation is considered fire-sensitive, i.e., not capable of adapting to natural fire regimes, and where fire disrupts the ecosystem [47]. However, according to our results, this formation is positively related to the intensity of fire activity in the Pantanal, which may be due to a combination of factors, such as recurrent droughts, human activities, and the lack of environmental policies to cope with illegal fires [49], for example.

Regarding the precision parameters trend ($1/\eta_\mu$), seasonality ($1/\eta_s$), and cycle ($1/\eta_c$), they cannot be directly interpreted, and are better interpreted through the time series of the posterior distribution of these components as shown in Figure 5. Thus, we decided to focus on the interpretation of the figures with the time series containing the posterior averages (solid lines) and the estimated 95% Bayesian credibility intervals (shaded areas) for each component. These components are interpreted as the contribution to the log-intensity function of the process for each period in time.

In the trend component (Figure 5a), we can observe a constant growth between 1998 and 2005, a rapid reduction between 2005 and 2008, with a stabilization in the values of the trend between 2008 and 2014. From 2015 until 2023, we can see two peaks, with the most significant between 2018 and 2021. Finally, at the end of the observed period, the trend reverts to a lower average level between 1998 and 2022.

The estimated seasonal component (Figure 5b) is quite stable, and the model does not indicate relevant changes in this pattern; that is, the estimated component captures a consistent seasonal pattern over the observed years.

Regarding the cyclical component (Figure 5c), it is important to note that it has stable behavior over time. This component has the capability to capture aperiodic changes that deviate from the mean, such as climatic anomalies, for example. Additionally, the estimated cycle parameter indicates low persistence in this component, with low values of partial autocorrelations (PAF1 and PACF2; see Table 2), but with a relevant variance over time, as shown in Figure 5.

The parameters Log τ , Log κ, and Group Φ are linked to the representation of the Matérn spatial covariance matrix used in the representation of the model, which is also better interpreted by the posterior distribution of the spatial random effect, shown in Figure 6. It is important to note that the temporal persistence of the spatial effect is relatively low, with Group Φ parameter estimated with a posterior mean value of 0.345, indicating a persistence in the spatial patterns of fire occurrence in the Pantanal.

The quarterly spatial heterogeneity of the fire events over 1998 and 2022 in the Brazilian Pantanal is clearer through the estimated spatial random effects (see Figure 6), which capture the observed variability of dry (with higher risk of fire occurrence) and wet periods in the region, with higher variability in the most fire-susceptible areas, i.e., mainly in the south and central areas, but also in the northeast and north portion of the Pantanal.

In Figure 6, we can see that the variability in the occurrence of fires is not homogeneous in time and space. For example, in 2001, 2009, 2012, and 2015, we observe a greater intensity in the southern region of the Pantanal, whereas in the period of record fires in 2020 there was a greater intensity in almost the entire area of the Pantanal, with emphasis on the northern region in the third quarter of 2020.

Figure 7 shows the predicted values for the model for the log intensity of the LGCP process, between 1998 and 2022. The adjusted intensity function reflects the sum of the effects of covariates, trend components, seasonality, and cycle and the spatial effects estimated by the model. We can observe that this function adequately explains the variations observed in the occurrences of fires in each quarter of the sample, in particular the periods with the record of occurrences of events in 2005Q3, 2007Q3 and 2020Q3.

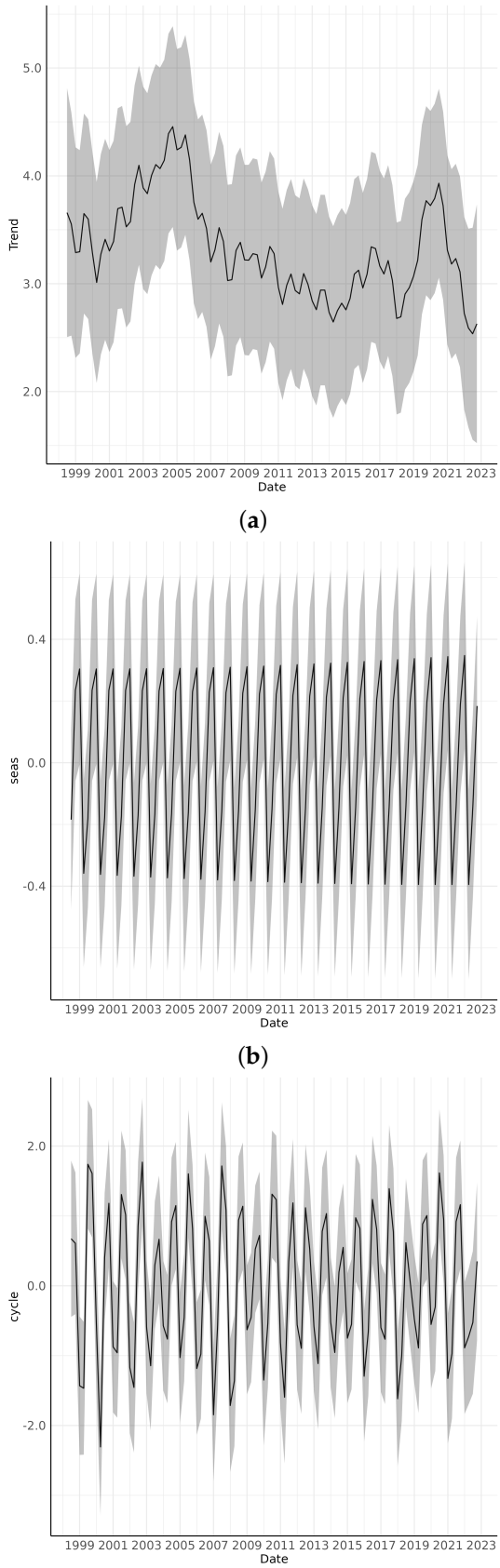

Figure 5. Trend, seasonal, and cycle decomposition of fire occurrences in the Brazilian Pantanal. (**a**) Trend, (**b**) seasonal, (**c**) cycle.

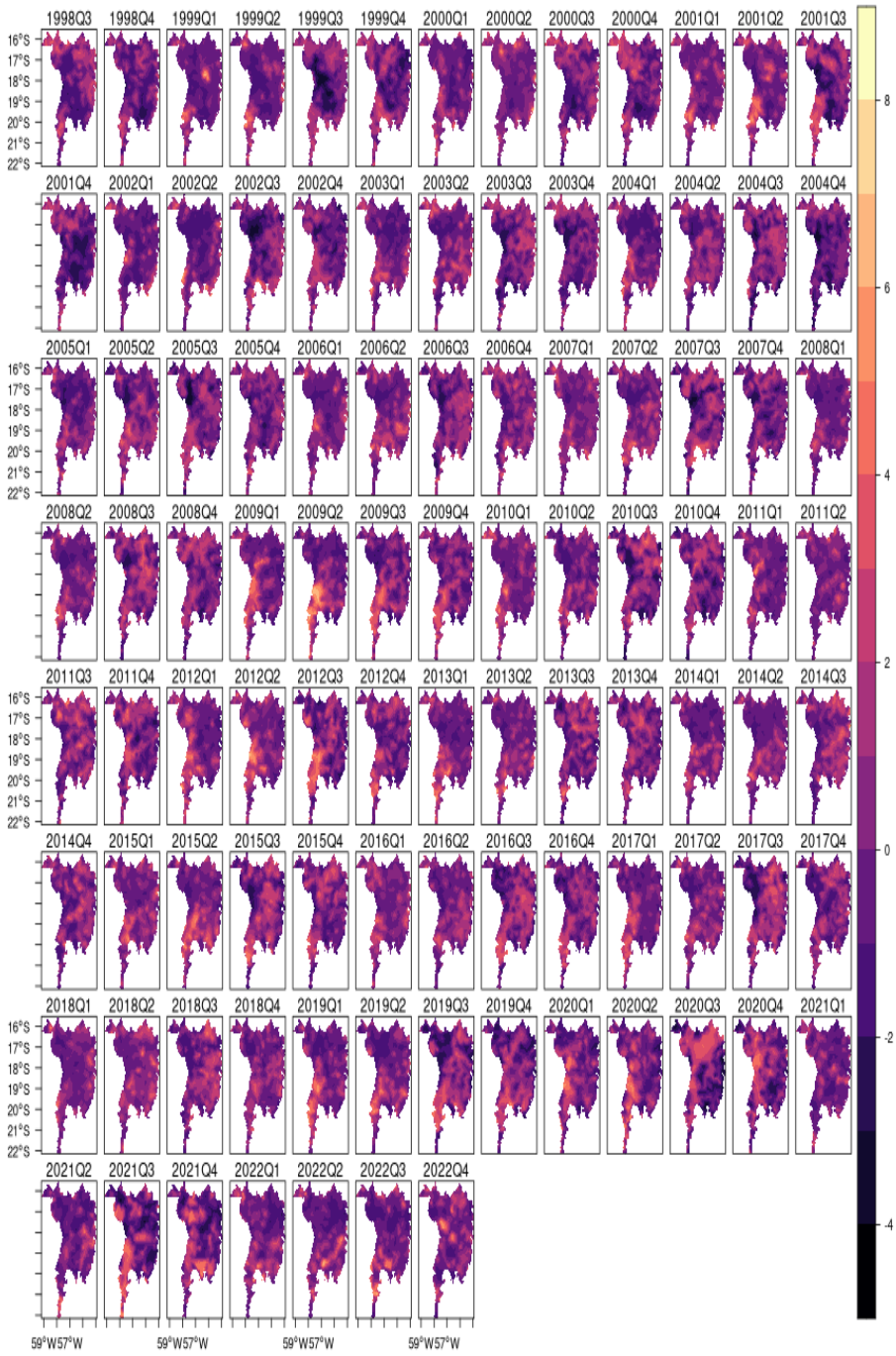

Figure 6. Spatial random effects. The figure shows the Bayesian estimation of the posterior mean of spatial random effects, for each period (quarter) in the sample, summarizing the spatial effects estimated by the model.

The spatiotemporal model proposed in this study is based on a separability structure between time and space and, despite the fact that this is quite a flexible structure, it is possible to have an alternative form using a non-separable structure for the interaction between time and space, allowing for a more complex dependency structure [19]. In this context, in the Appendix A.3, we provide a non-separable version of our spatiotemporal model, which allows us to analyze a more complex dependency structure, despite the computational cost involved in this type of analysis. The Appendix A.3 presents the mesh used in this analysis (Figure A1), the estimated parameters (Table A1), the estimated trend,

cycle, and seasonality components (Figure A2), and the spatial random effects obtained with this representation (Figure A3). The results obtained with the non-separable model are similar to those of the separable model, indicating the robustness of the results in relation to the separability assumption.

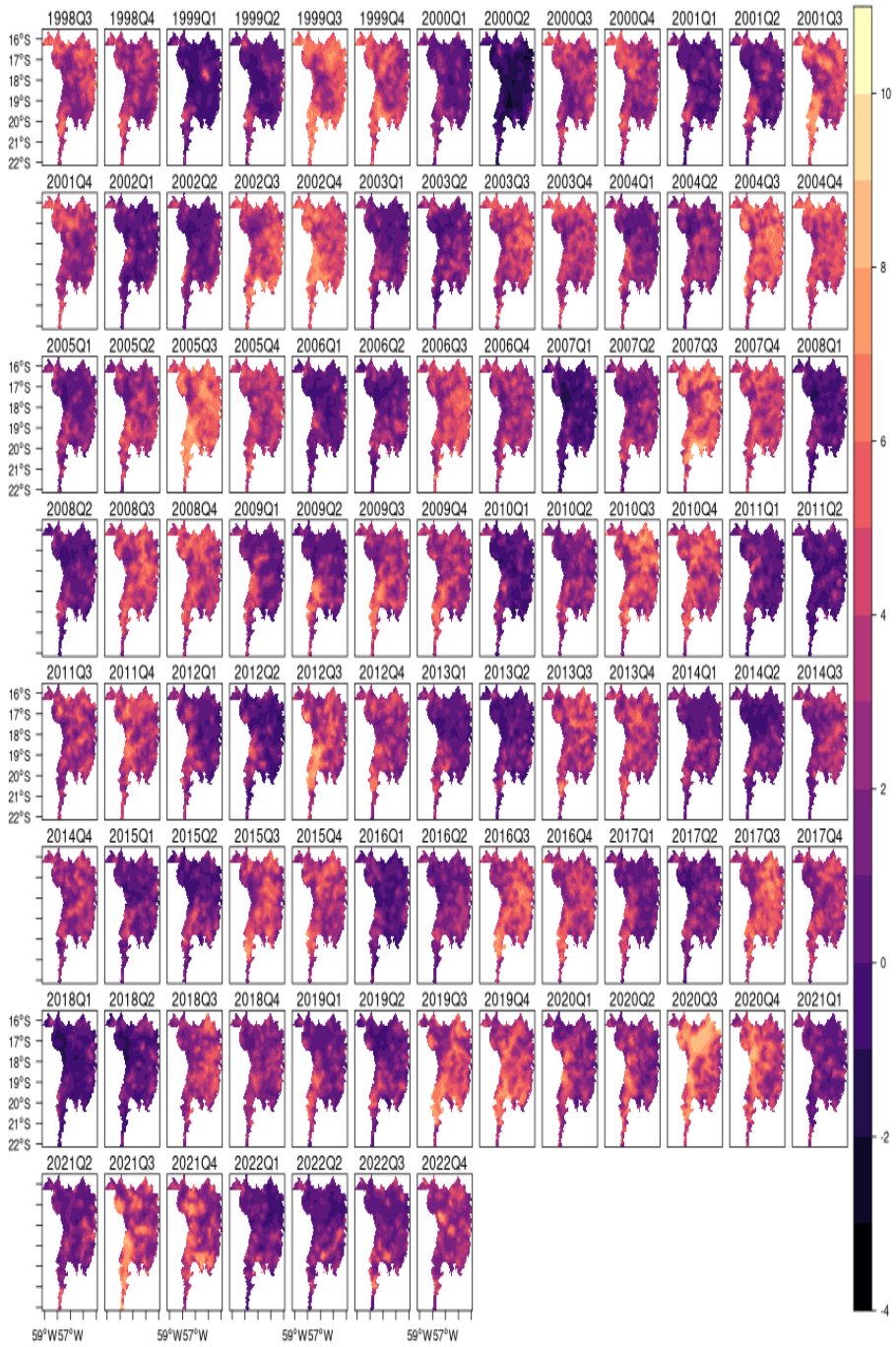

Figure 7. Fitted log intensity . The figure shows the Bayesian estimation of the posterior mean of the log-intensity function of the spatial point process for each period (quarter) in the sample. The log-intensity function is given by the sum of the trend, seasonality, and cycle components and the effect of covariates in the model.

6. Conclusions

To assess changes in fire occurrence patterns in the Brazilian Pantanal, we propose using a dynamic version of a Log-Gaussian Cox process. This approach decomposes the intensity function into latent components such as trend, seasonality, cycles, covariates, and spatial effects. It enables us to identify long-term changes in occurrence intensity over time and capture mean-reverting effects, while also accounting for spatial heterogeneity.

Statistically significant covariates included rainfall, represented by accumulated rainfall per quarter, and land use/cover variables specific to each analyzed location. Regarding the included covariates, our results are consistent with other studies that analyzed changes in the pattern of fires in the Pantanal and the potential climatic and anthropogenic causes of these changes.

In particular, we observed a statistically significant increase in fire incidence in natural vegetation areas, consistent with the results of [28,29], and especially with the results of [31] that demonstrate a preference for forest regions during the 2020 fires, with forests and grasslands experiencing larger fire patches compared to crops, consistent with previous results from [32].

Additionally, our findings support the evidence that rainfall patterns play a crucial role in explaining the heterogeneity in fire occurrence. This aligns with the findings of [24], which highlight severe drought, extreme temperatures, and increased fuel availability as key factors contributing to the record number of fires in 2020.

Regarding the estimated latent components, within the proposed framework, our findings suggest the existence of a variability in the trend component, which exhibits a growth pattern between 1998 and 2005, and after 2019, whereas it remained relatively stable between 2008 and 2019. On the other hand, seasonal and cycle estimated components have stable behaviors over time.

The model presented in this work represents a new tool for statistical monitoring of changes in the fire pattern. It allows the decomposition of variations observed in time and space into permanent (trend) and transitory (seasonal and cyclical) components, controlling climatic causes and patterns of land use and cover, and can be applied in real time using the information obtained by remote sensing of fire occurrences.

We can enumerate the main contributions of our analysis:

1. Dynamic Spatiotemporal Modeling: We propose a dynamic modeling approach to monitor fire occurrence patterns in the Brazilian Pantanal. This method involves modeling the dynamics of point processes of geolocated events (fire spots) using remote sensing data, through a spatiotemporal decomposition for the period 1999–2022.
2. Incorporation of Flexible Statistical Methodology: Our approach employs a dynamic version of a Log-Gaussian Cox Process (LGCP), which decomposes the intensity function into latent components such as trend, seasonality, cycles, covariates, and spatial effects. This novel methodology builds upon previous research and incorporates time-varying spatial effects based on an autoregressive functional structure.
3. Comprehensive Understanding of Fire Patterns: By integrating remote sensing technology with statistical modeling, our methodology provides a robust framework for assessing and predicting fire occurrences in the Pantanal. It enables a comprehensive understanding of fire patterns over time and space, contributing to the advancement of environmental science research.
4. Contribution to Environmental Science Research: Our modeling approach provides a robust foundation for investigating potential anthropogenic factors contributing to the spatiotemporal distribution of fires in the Pantanal. It offers insights into the underlying dynamics of fire occurrences, aiding in the identification of factors driving changes in fire patterns.
5. Consistency with Previous Studies: Our results align with other studies analyzing changes in fire patterns in the Pantanal and the possible climatic and anthropogenic causes of these changes. We corroborate the importance of factors such as rain-

fall patterns and land cover/use in explaining the heterogeneity and intensity of fire occurrences.

6. Tool for Statistical Monitoring: The model presented in our work represents a new tool for statistical monitoring of changes in fire patterns. It allows for the decomposition of variations observed in time and space into permanent and transitory components while controlling for climatic causes and patterns of land use and cover.
7. Real-time Application and Integration with INPE's Queimadas System: Our model offers a direct application as a complementary analysis tool to INPE's Queimadas system data. Integrating estimations of trend, seasonality, and cycle components enhances the system's data summaries and aids in elucidating statistical patterns and overall trends in spatiotemporal data. Additionally, utilizing spatial random effects enables visualization of shifts in the spatial occurrence patterns of fires, augmenting the analytical capabilities of the Queimadas system.

Author Contributions: Conceptualization, F.V. and M.L.; methodology, F.V. and M.L.; formal analysis, F.V. and M.L.; investigation, F.V. and M.L.; writing—original draft preparation, F.V. and M.L.; writing—review and editing, F.V. and M.L. All authors have read and agreed to the published version of the manuscript.

Funding: The authors acknowledge funding from Instituto Escolhas, CNPq (310646/2021-9) and FAPESP (2023/02538-0).

Institutional Review Board Statement: Not applicable.

Informed Consent Statement: Not applicable.

Data Availability Statement: Main data taken from Sistema Queimadas https://terrabrasilis.dpi.inpe.br/queimadas/bdqueimadas/, accessed on 31 December 2022, and MapBiomas https://mapbiomas.org, accessed on 31 December 2022.

Conflicts of Interest: The authors declare no conflicts of interest.

Abbreviations

ANA: Agência Nacional de Águas. AR: Autoregressive. AVHRR: Advanced Very High Resolution Radiometer. FAO: Food and Agriculture Organization. GMRF: Gaussian Markov random field. IBGE: Instituto Brasileiro de Geografia e Estatística. INMET: Instituto Nacional de Metereologia. LGCP: Log-Gaussian Cox Process. LULC: Land Use and Land Cover. MODIS: Moderate Resolution Imaging Spectroradiometer. NOAA: National Oceanic and Atmospheric Administration. PACF: Partial autocorrelation function. SPDE: Stochastic partial differential equation. UMD: University of Maryland. UPRB: Upper Paraguay River Basin. Y_t—Observed points in period t. Ω—Region under analysis. $\lambda(s,t)$—Intensity Function in location s and period t. μ_t—trend in period t. s_t—seasonal in period t. c_t—cycle in period t. $z(s,t)$—covariate in location s and period t. $\xi(s,t)$—spatial effects location s and period t. θ_i—parameter for cycle component of order i. η_μ—variance of trend. η_s—variance of seasonal. η_c—variance of cycle. $\omega(s,t)$—Gaussian component location s and period t. β—parameter for covariates. $C(h)$—covariance function of the Matérn class τ—range parameter of covariance function. κ—spatial scale parameter of covariance function. ν—smoothness parameter of covariance function. $K_{\_}$—modified Bessel function. Φ—Group parameter of covariance function.

Appendix A

Appendix A.1. LGCP Likelihood Approximation

The method proposed by [21] is based on constructing an approximation to the intractable likelihood function for a LGCP process with a stochastic intensity function in the form

$$\pi(Y \mid \lambda) = \exp\left\{ |\Omega| - \int_\Omega \lambda(s)\, ds \right\} \prod_{s_i \in Y} \lambda(s_i). \tag{A1}$$

The main idea is to construct a continuously specified random field using a basis expansion, as follows:

$$Z(s) = \sum_{i=1}^{n} z_i \phi_i(s), \tag{A2}$$

with $z = (z_1, \ldots, z_n)^T$ being a multivariate Gaussian random vector and $\{\phi_i(s)\}_{i=1}^n$ is a set of linearly independent deterministic basis functions. The log-likelihood $\log \pi(y \mid Z) = |\Omega| - \int_\Omega \exp\{Z(s)\}\, ds + \sum_{i=1}^N Z(s_i)$ is the sum of two components: the stochastic integral, and the field evaluated at the data points. Using a deterministic integration rule $\int_\Omega f(s)\, ds \approx \sum_{i=1}^p \tilde{\alpha}_i f(\tilde{s}_i)$, for fixed nodes $\{\tilde{s}_i\}_{i=1}^p$ and weights $\{\tilde{\alpha}_i\}_{i=1}^p$, ref. [21] proposed the approximation

$$\begin{aligned} \log\{\pi(y \mid z)\} &\approx C - \sum_{i=1}^{p} \tilde{\alpha}_i \exp\left\{ \sum_{j=1}^{n} z_j \phi_j(\tilde{s}_i) \right\} + \sum_{i=1}^{N} \sum_{j=1}^{n} z_j \phi_j(s_i) \\ &= C - \tilde{\alpha}^T \exp(A_1 z) + 1^T A_2 z, \end{aligned} \tag{A3}$$

with C as a constant, $[A_1]_{ij} = \phi_j(\tilde{s}_i)$ as a matrix containing the values of the latent Gaussian model (A2) at the integration nodes $\{\tilde{s}_i\}$, and $[A_2]_{ij} = \phi_j(s_i)$ evaluates the latent Gaussian field at the observed points $\{s_i\}$. As discussed by [21], the main advantage of the approximation (A3) follows a Poisson representation. Given z and θ, the approximate likelihood is composed of $N + p$-independent Poisson random variables. To show this property, ref. [21] write $\log \eta = (z^T A_1^T, z^T A_2^T)^T$ and $\alpha = (\tilde{\alpha}^T, 0_{N\times 1}^T)^T$. For pseudo-observations $y = (0_{p\times 1}^T, 1_{N\times 1}^T)^T$, the approximate likelihood factors are given by

$$\pi(y \mid z) \approx C \prod_{i=1}^{N+p} \eta_i^{y_i} e^{-\alpha_i \eta_i}, \tag{A4}$$

which is analogous to the likelihood for observing $N + p$ conditionally independent Poisson random variables with means $\alpha_i \eta_i$ and observed values y_i. The properties of this approximation are discussed in [21]. The essential results about the convergence properties of the approximations for the stochastic integral and the random field are demonstrated in Section 4 and the Appendix of [21].

Our parameterization is based on decomposing the random field representation of the intensity function of a spatiotemporal LGCP as the composition of the static representation of for each period t, and in each period the log-intensity function is given by the sum of the common latent components of trend, seasonality and cycle and the effects of covariates, given by Equation (2). The random field generated by intensity function of the LGCP approach of [21] is represented using the SPDE framework of [42]. We describe this method in the next section.

Appendix A.2. The Spatial Covariance Function and Model Details

In this section, we provide a brief description of the SPDE approach proposed by [42]. The spatial structure of the model is given by the Matérn family, as discussed in the section Data and Methods. The marginal variance of the covariance function σ^2 is given by the following:

$$\sigma^2 = \frac{\Gamma(\nu)}{4\pi\kappa^{2\nu}\tau^2\Gamma(\nu + \frac{d}{2})} \tag{A5}$$

where τ is a scaling parameter and d is the space dimension. In order to easier obtain the results, we adopt a parameterization in terms of $\log \tau$ and $\log \kappa$ for the covariance function, following [42]:

$$\log \tau = \frac{1}{2}\log\left(\frac{\Gamma(\nu)}{\Gamma(\alpha)(4\pi)^{d/2}}\right) - \log\sigma - \nu\log\rho$$
$$\log \kappa = \frac{\log(8\nu)}{2} - \log\rho \tag{A6}$$

where $\rho = \frac{(8\nu)^{1/2}}{\kappa}$. To approximate the LGCP likelihood, we adopt SPDE approach, using the fact that the term $\omega(s,t)$ corresponds to a random field with a Matérn covariance, which allows to approximate this structure with a Gaussian Markov Random Field (GMRF).

Thus, the first main result for the SPDE approach, is that the GF $\omega(s)$ with the Matérn covariance function is a stationary solution to the linear fractional SPDE [42,50]:

$$(\kappa - \Delta)^{\alpha/2} x(s) = W(s), \quad s \in R^d, \quad \alpha = \nu + d/2, \quad \kappa > 0, \quad \nu > 0 \tag{A7}$$

where $\Delta = \sum_{i=1}^{d} \frac{\partial^2}{\partial s_i^2}$ is the Laplacian operator and $W(s)$ is a spatial white noise. Therefore, in order to find a GMRF approximation of a GF, we need to find the stochastic weak solution of SPDE (A7). Using the Finite Elements Method (FEM), it is possible to construct an approximated solution of SPDE [42], which is given by

$$x(s,t) \approx \tilde{x}(s,t) = \sum_{j=1}^{n} w_j \varphi_j(s,t) \tag{A8}$$

where n is the number of vertices of the triangulation, $\{w_j\}_{j=1}^{n}$ are the weights with Gaussian distribution, and $\{\varphi_j\}_{j=1}^{n}$ are the basis functions defined for each node on the mesh. In summary, the idea is to calculate the weights $\{w_j\}$, which determine the values of the field at the vertices, whereas the values inside the triangles are determined by linear interpolation [42], and Equation (A8) represents a link between the GF and GMRF, where $\{\omega_j\}$ has a Markovian structure [42].

By replacing the GF by the GMRF approximation, we obtain an approximation of the LGCP likelihood, which consists of $(n + n_t)T$ independent Poisson random variables, where n is the number of vertices and n_t is the number of observed fires [21]. Under the GMRF structure, it is possible to estimate the model within the Bayesian framework using the Integrated Nested Laplace Approximation (INLA) framework, which allows the use of deterministic approximations to perform the estimation of latent parameters and components in models with an additive structure. A more detailed description of the INLA method can be found in [45]. In all analyses, we use the standard reference prior structure described in [51]. We use log-gamma priors for the precision parameters of the trend and seasonal components, and penalized complexity priors for the precision and the autoregressive parameters of the cycle components, Gaussian priors for the parameters of covariates, and a multivariate Gaussian prior for the parameters of the Matérn covariance function. Details can be obtained from the authors.

Appendix A.3. Non-Separable Spatiotemporal Model

The model proposed in this paper assumes a separable structure between the spatial and temporal effects, assuming a Kronecker product between the spatial and temporal covariances to obtain the spatiotemporal representation, which is advantageous due to its flexibility. Despite the computational cost, by assuming a non-separable structure for time and space, it is possible to analyze a more complex dependency structure. In order to provide an additional robustness analysis, we estimated a non-separable version of the proposed model presented in the previous section, following [52], which provides a non-separable representation for the spatiotemporal random effects using the generalization of the Matérn covariance structure. In particular, in this representation the structure of the

spatiotemporal random effects is given by a diffusion-based extension of the Matérn field, i.e., the random field $u(s,t)$ can be written as

$$\left(\gamma_t \frac{d}{dt} + L^{\alpha_s/2}\right)^{\alpha_t} u(s,t) = \mathcal{E}_Q(s,t) \tag{A9}$$

with $L = \gamma_s^2 - \Delta$, $\mathcal{E}_Q(s,t)$ being Gaussian noise that is white in time but correlated, with precision operator $Q(\gamma_s, \gamma_\epsilon, \alpha_\epsilon) = \gamma_\epsilon^2 L^{\alpha_\epsilon}$, with $(\gamma_t, \gamma_s, \gamma_e)$ being fixed scaling parameters, and $(\alpha_t, \alpha_s, \alpha_e)$ parameters in the model.

Defining $\alpha = \alpha_e + \alpha_s(\alpha_t - 1/2)$, and assuming that $\alpha_t, \alpha_s, \alpha_e$ satisfy $\alpha > 1$, the solution $u(s,t)$ has marginal spatial covariance function given by the following:

$$C(u(t,s_1), u(t,s_2)) = \frac{\sigma^2}{\Gamma(\nu_s)2^{\nu-1}} (\gamma_s \|s_1 - s_2\|)^{\nu_s} K_{\nu_s}(\gamma_s \|s_1 - s_2\|), \tag{A10}$$

where $\nu_s = \alpha - 1$ and

$$\sigma^2 = \frac{\Gamma(\alpha_t - 1/2)\Gamma(\alpha - 1)}{\Gamma(\alpha_t)\Gamma(\alpha)8\pi^{3/2}\gamma_e^2\gamma_t\gamma_s^{2(\alpha-1)}}. \tag{A11}$$

In order to carry out our analysis, we estimate a non-separable version of our LGCP model, replacing the random field structure, $\xi(s,t)$, of the model defined in 2, with the random field $u(s,t)$ previously defined.

We also assume the parametrization of the parameters defining σ, r_s, r_t as:

$$\begin{aligned} c_1 &= \frac{\Gamma(\alpha_t - 1/2)\Gamma(\alpha - 1)}{\Gamma(\alpha_t)\Gamma(\alpha)4\sqrt{\pi}} \\ \sigma &= \gamma_\epsilon^{-1} c_1^{1/2} \gamma_t^{-1/2} \gamma_s^{-(\alpha-1)} \\ r_s &= \gamma_s^{-1}\sqrt{8\nu_s} \\ r_t &= \gamma_t \sqrt{8(\alpha_t - 1/2)}\gamma_s^{-\alpha_s}, \end{aligned} \tag{A12}$$

and the model is estimated using parameters $\log\sigma$, $\log r_s$, $\log r_t$. Due to the higher computational cost and memory limitations in representing the model with the non-separable structure, we estimate the model with an alternative mesh with a lower resolution than the separable model, shown in Figure A1, with the same prior previously defined for the estimation of the model (2), and also adopting the INLA approximations to perform the Bayesian inference procedures. The estimated posterior distribution of parameters in the non-separable spatiotemporal LGCP model is presented in Table A1, the estimated latent components of trend, seasonal and cycle components in Figure A2, and the non-separable spatiotemporal random effect is presented in Figure A3.

The results of the estimated non-separable spatiotemporal model indicate similar effects for the covariates in relation to those obtained in the model with the separable spatial random effects. Additionally, this model was able to capture a wider range of values for the random effects when compared to those estimated by the separable model, as can be seen in Figure A3. Regarding the estimated components, in Figure A2, it is possible to observe that the non-separable model was able to capture an increase in the trend component during 2019 and 2020, when the historical fires occurred in the Pantanal biome. Despite that, the estimated cycle and seasonal components presented similar patterns to those obtained by the model with the separable structure.

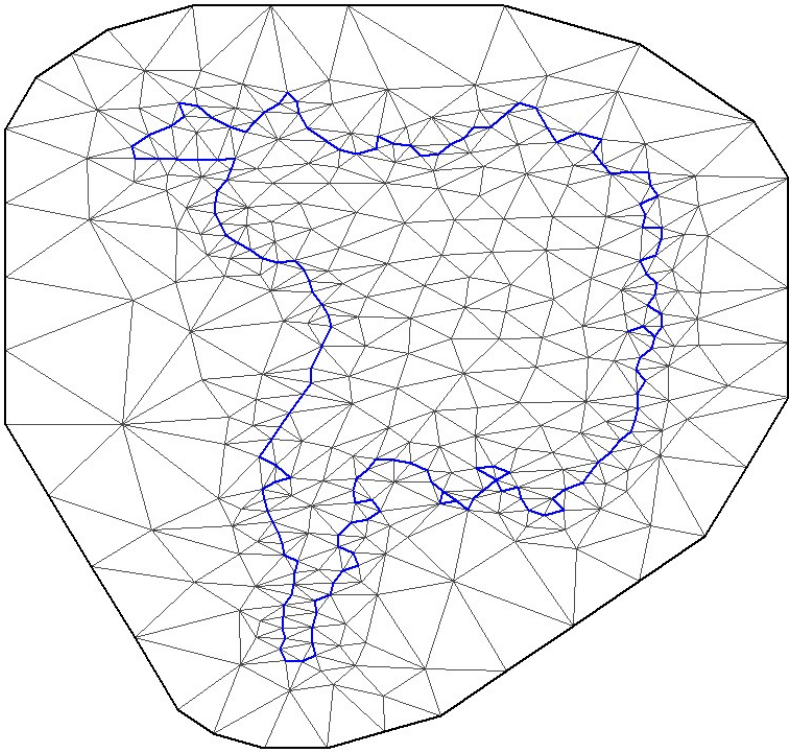

Figure A1. Spatial mesh of the Brazilian Pantanal—non-separable spatiotemporal model.

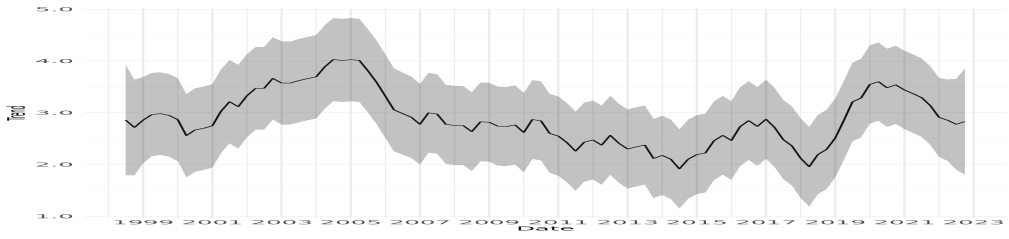

(**a**)

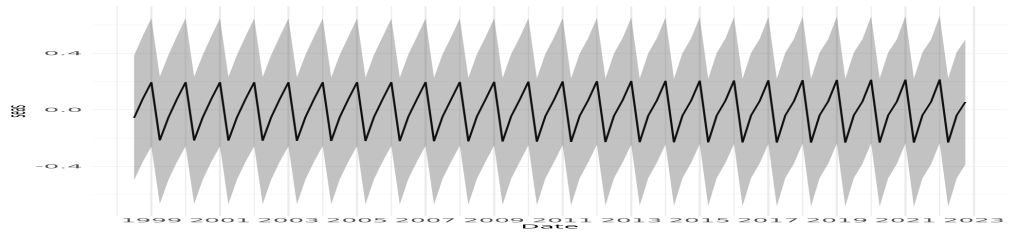

(**b**)

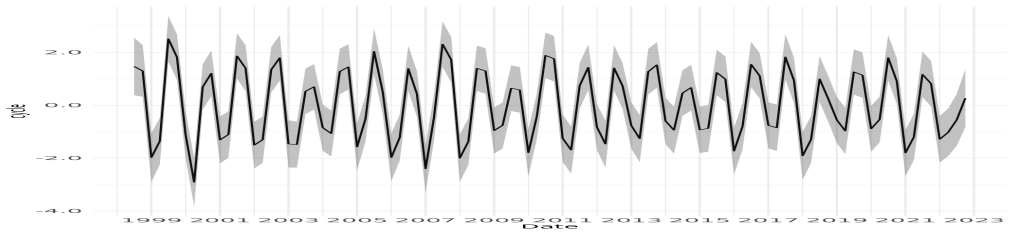

(**c**)

Figure A2. Trend, seasonal, and cycle decomposition of fire occurrences in the Brazilian Pantanal—non-separable spatiotemporal model. (**a**) Trend, (**b**) seasonal, (**c**) cycle.

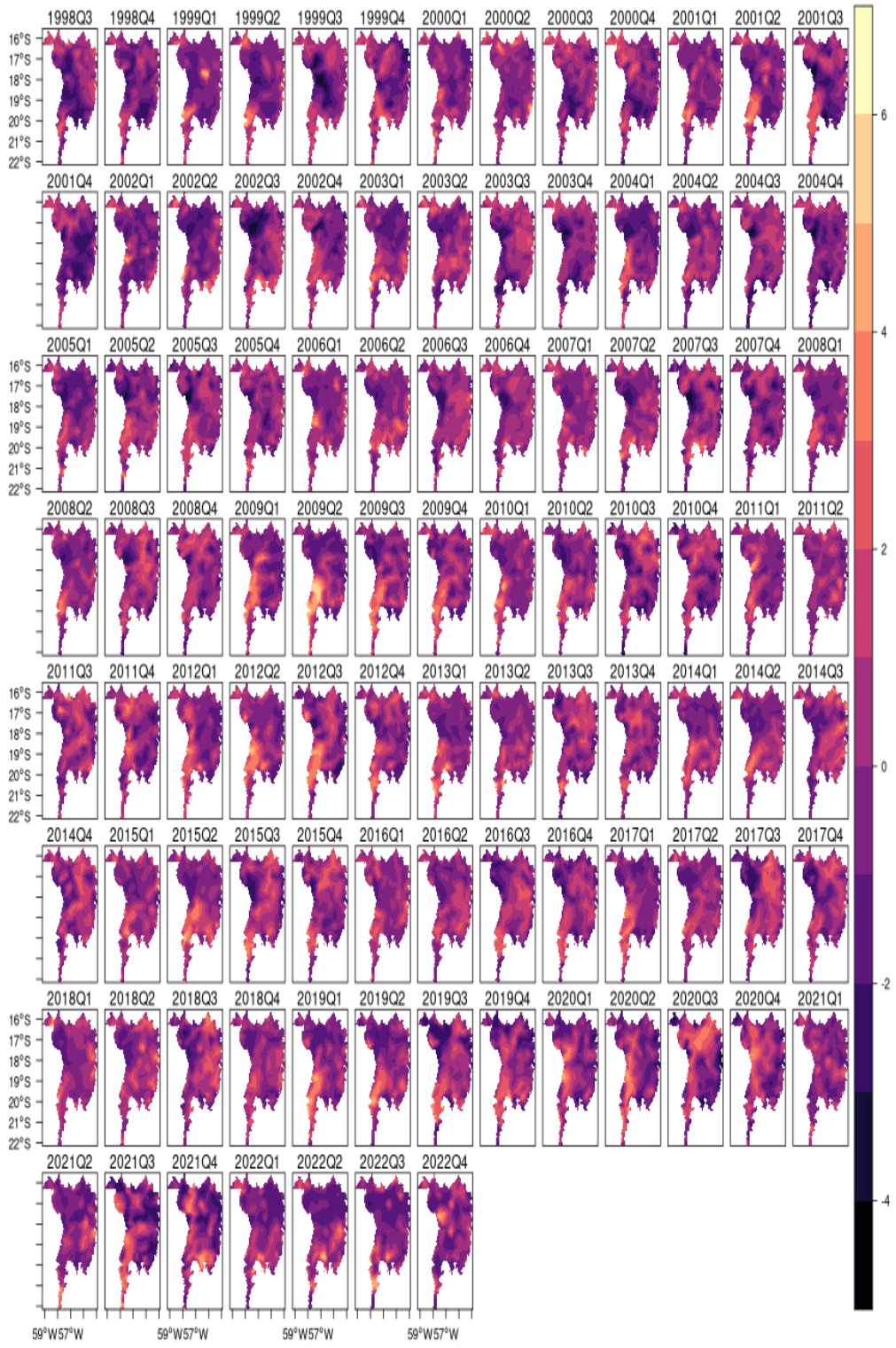

Figure A3. Spatial random effects—non-separable spatiotemporal model. The figure shows the Bayesian estimation of the posterior mean of spatial random effects, for each period (quarter) in the sample, summarizing the spatial effects estimated by the model.

Table A1. Estimated parameters —non-separable spatiotemporal model.

	Mean	SD	0.025 Quant	0.5 Quant	0.975 Quant	Mode
Fixed effects						
Rainfall	−0.001	0.000	−0.001	−0.001	0.000	−0.001
Forest formation	0.148	0.044	0.062	0.148	0.235	0.148
Savanna formation	0.186	0.049	0.090	0.186	0.283	0.186
Grassland formation	0.295	0.049	0.199	0.295	0.391	0.295
Random effects						
Precision for trend	6.048	0.278	5.539	6.038	6.686	6.003
Precision for seasonality	11,785.288	710.372	10,312.207	11,752.653	13,245.996	11,827.200
Precision for cycle	0.817	0.031	0.750	0.816	0.880	0.819
PACF1 for cycle	0.077	0.013	0.050	0.077	0.105	0.077
PACF2 for cycle	−0.585	0.007	−0.598	−0.585	−0.569	−0.586
$\log \sigma$	0.973	0.044	0.887	0.973	1.063	0.972
$\log r_s$	−0.980	0.010	−1.000	−0.980	−0.959	−0.981
$\log r_t$	0.599	0.003	0.592	0.599	0.606	0.599

References

1. Wantzen, K.M.; Assine, M.L.; Bortolotto, I.M.; Calheiros, D.F.; Campos, Z.; Catella, A.C.; Chiaravalotti, R.M.; Collischonn, W.; Couto, E.G.; Nunes da Cunha, C.; et al. The Pantanal Wetland Menaced by the Hidrovia Navigation Project: The End of an Entire Biome? Technical Report. 2023. Available online: https://ssrn.com/abstract=4510907 (accessed on 31 December 2023).
2. da Silva, J.d.S.V.; de Moura Abdon, M. Delimitação do Pantanal brasileiro e suas sub-regiões. *Pesqui. Agropecuária Bras.* **1998**, *33*, 1703–1711.
3. Tomas, W.M.; de Oliveira Roque, F.; Morato, R.G.; Medici, P.E.; Chiaravalloti, R.M.; Tortato, F.R.; Penha, J.M.; Izzo, T.J.; Garcia, L.C.; Lourival, R.F.; et al. Sustainability agenda for the Pantanal wetland: Perspectives on a collaborative Interface for science, policy, and decision-making. *Trop. Conserv. Sci.* **2019**, *12*. [CrossRef]
4. Harris, M.B.; Tomas, W.; Mourão, G.; Da Silva, C.J.; Guimaraes, E.; Sonoda, F.; Fachim, E. Safeguarding the Pantanal wetlands: Threats and conservation initiatives. *Conserv. Biol.* **2005**, *19*, 714–720. [CrossRef]
5. Silva, J.; Abdon, M.d.M.; da Silva, S.M.A.; de Moraes, J.A. Evolution of deforestation in the Brazilian Pantanal and surroundings in the timeframe 1976–2008. *Geografia* **2011**, *36*, 35–55.
6. Arvor, D.; Meirelles, M.; Dubreuil, V.; Begue, A.; Shimabukuro, Y.E. Analyzing the agricultural transition in Mato Grosso, Brazil, using satellite-derived indices. *Appl. Geogr.* **2012**, *32*, 702–713. [CrossRef]
7. Instituto SOS Pantanal; WWF-Brasil. Monitoramento das Alterações da Cobertura Vegetal e uso do Solo na Bacia do Alto Paraguai–Porção Brasileira. Período de Análise: 2012–2014. 2015. Technical Report. 2020. Available online: https://www.wwf.org.br/?25181/Monitoramento-das-alteracoes-da-cobertura-vegetal-e-uso-do-solo-na-Bacia-do-Alto-Paraguai (accessed on 31 January 2023).
8. Ivory, S.J.; McGlue, M.M.; Spera, S.; Silva, A.; Bergier, I. Vegetation, rainfall, and pulsing hydrology in the Pantanal, the world's largest tropical wetland. *Environ. Res. Lett.* **2019**, *14*, 124017. [CrossRef]
9. de Oliveira, M.T.; Damasceno-Junior, G.A.; Pott, A.; Paranhos Filho, A.C.; Suarez, Y.R.; Parolin, P. Regeneration of riparian forests of the Brazilian Pantanal under flood and fire influence. *For. Ecol. Manag.* **2014**, *331*, 256–263. [CrossRef]
10. Arruda, W.d.S.; Oldeland, J.; Paranhos Filho, A.C.; Pott, A.; Cunha, N.L.; Ishii, I.H.; Damasceno-Junior, G.A. Inundation and fire shape the structure of riparian forests in the Pantanal, Brazil. *PloS ONE* **2016**, *11*, e0156825. [CrossRef]
11. Junk, W.J.; Da Cunha, C.N.; Wantzen, K.M.; Petermann, P.; Strüssmann, C.; Marques, M.I.; Adis, J. Biodiversity and its conservation in the Pantanal of Mato Grosso, Brazil. *Aquat. Sci.* **2006**, *68*, 278–309. [CrossRef]
12. Guerra, A.; de Oliveira Roque, F.; Garcia, L.C.; Ochoa-Quintero, J.M.; de Oliveira, P.T.S.; Guariento, R.D.; Rosa, I.M. Drivers and projections of vegetation loss in the Pantanal and surrounding ecosystems. *Land Use Policy* **2020**, *91*, 104388. [CrossRef]
13. Guerra, A.; de Oliveira, P.T.S.; de Oliveira Roque, F.; Rosa, I.M.; Ochoa-Quintero, J.M.; Guariento, R.D.; Colman, C.B.; Dib, V.; Maioli, V.; Strassburg, B.; et al. The importance of Legal Reserves for protecting the Pantanal biome and preventing agricultural losses. *J. Environ. Manag.* **2020**, *260*, 110128. [CrossRef] [PubMed]
14. Costanza, R.; d'Arge, R.; De Groot, R.; Farber, S.; Grasso, M.; Hannon, B.; Limburg, K.; Naeem, S.; O'neill, R.V.; Paruelo, J.; et al. The value of the world's ecosystem services and natural capital. *Nature* **1997**, *387*, 253–260. [CrossRef]
15. Seidl, A.F.; Moraes, A.S. Global valuation of ecosystem services: Application to the Pantanal da Nhecolandia, Brazil. *Ecol. Econ.* **2000**, *33*, 1–6. [CrossRef]
16. Costanza, R.; De Groot, R.; Sutton, P.; Van der Ploeg, S.; Anderson, S.J.; Kubiszewski, I.; Farber, S.; Turner, R.K. Changes in the global value of ecosystem services. *Glob. Environ. Chang.* **2014**, *26*, 152–158. [CrossRef]
17. Laurini, M. A spatio-temporal approach to estimate patterns of climate change. *Environmetrics* **2019**, *30*, e2542. [CrossRef]

18. Valente, F.; Laurini, M. Tornado Occurrences in the United States: A Spatio-Temporal Point Process Approach. *Econometrics* **2020**, *8*, 25. [CrossRef]
19. Valente, F.; Laurini, M. Pre-harvest sugarcane burning: A statistical analysis of the environmental impacts of a regulatory change in the energy sector. *Clean. Eng. Technol.* **2021**, *4*, 100255. [CrossRef]
20. Valente, F.; Laurini, M. Spatio-temporal analysis of fire occurrence in Australia. *Stoch. Environ. Res. Risk Assess.* **2021**, *35*, 1759–1770. [CrossRef]
21. Simpson, D.; Illian, J.B.; Lindgren, F.; Sørbye, S.H.; Rue, H. Going off grid: Computationally efficient inference for log-Gaussian Cox processes. *Biometrika* **2016**, *103*, 49–70. [CrossRef]
22. Schulz, C.; Whitney, B.S.; Rossetto, O.C.; Neves, D.M.; Crabb, L.; de Oliveira, E.C.; Lima, P.L.T.; Afzal, M.; Laing, A.F.; de Souza Fernandes, L.C.; et al. Physical, ecological and human dimensions of environmental change in Brazil's Pantanal wetland: Synthesis and research agenda. *Sci. Total Environ.* **2019**, *687*, 1011–1027. [CrossRef]
23. Garcia, L.C.; Szabo, J.K.; de Oliveira Roque, F.; de Matos Martins Pereira, A.; Nunes da Cunha, C.; Damasceno-Júnior, G.A.; Morato, R.G.; Tomas, W.M.; Libonati, R.; Ribeiro, D.B. Record-breaking wildfires in the world's largest continuous tropical wetland: Integrative fire management is urgently needed for both biodiversity and humans. *J. Environ. Manag.* **2021**, *293*, 112870. [CrossRef] [PubMed]
24. Libonati, R.; Geirinhas, J.L.; Silva, P.S.; Russo, A.; Rodrigues, J.A.; Belém, L.B.C.; Nogueira, J.; Roque, F.O.; DaCamara, C.C.; Nunes, A.M.B.; et al. Assessing the role of compound drought and heatwave events on unprecedented 2020 wildfires in the Pantanal. *Environ. Res. Lett.* **2022**, *17*, 015005. [CrossRef]
25. Libonati, R.; Geirinhas, J.L.; Silva, P.S.; Monteiro dos Santos, D.; Rodrigues, J.A.; Russo, A.; Peres, L.F.; Narcizo, L.; Gomes, M.E.R.; Rodrigues, A.P.; et al. Drought–heatwave nexus in Brazil and related impacts on health and fires: A comprehensive review. *Ann. N. Y. Acad. Sci.* **2022**, *1517*, 44–62. [CrossRef]
26. Silva, P.S.; Geirinhas, J.L.; Lapere, R.; Laura, W.; Cassain, D.; Alegría, A.; Campbell, J. Heatwaves and fire in Pantanal: Historical and future perspectives from CORDEX-CORE. *J. Environ. Manag.* **2022**, *323*, 116193. [CrossRef] [PubMed]
27. Menezes, L.S.; de Oliveira, A.M.; Santos, F.L.; Russo, A.; de Souza, R.A.; Roque, F.O.; Libonati, R. Lightning patterns in the Pantanal: Untangling natural and anthropogenic-induced wildfires. *Sci. Total Environ.* **2022**, *820*, 153021. [CrossRef] [PubMed]
28. Kumar, S.; Getirana, A.; Libonati, R.; Hain, C.; Mahanama, S.; Andela, N. Changes in land use enhance the sensitivity of tropical ecosystems to fire-climate extremes. *Sci. Rep.* **2022**, *12*, 964. [CrossRef]
29. Ribeiro, A.F.S.; Brando, P.M.; Santos, L.; Rattis, L.; Hirschi, M.; Hauser, M.; Seneviratne, S.I.; Zscheischler, J. A compound event-oriented framework to tropical fire risk assessment in a changing climate. *Environ. Res. Lett.* **2022**, *17*, 065015. [CrossRef]
30. Marques, J.F.; Alves, M.B.; Silveira, C.F.; Amaral e Silva, A.; Silva, T.A.; dos Santos, V.J.; Calijuri, M.L. Fires dynamics in the Pantanal: Impacts of anthropogenic activities and climate change. *J. Environ. Manag.* **2021**, *299*, 113586. [CrossRef]
31. Correa, D.B.; Alcântara, E.; Libonati, R.; Massi, K.G.; Park, E. Increased burned area in the Pantanal over the past two decades. *Sci. Total Environ.* **2022**, *835*, 155386. [CrossRef]
32. Ferreira Barbosa, M.L.; Haddad, I.; da Silva Nascimento, A.L.; Máximo da Silva, G.; Moura da Veiga, R.; Hoffmann, T.B.; Rosane de Souza, A.; Dalagnol, R.; Susin Streher, A.; Souza Pereira, F.R.; et al. Compound impact of land use and extreme climate on the 2020 fire record of the Brazilian Pantanal. *Glob. Ecol. Biogeogr.* **2022**, *31*, 1960–1975. [CrossRef]
33. Kingman, J.F.C. *Poisson Processes*; Clarendon Press: Oxford, UK, 1992.
34. Baddeley, A.; Rubak, E.; Turner, R. *Spatial Point Patterns: Methodology and Applications with R*; Chapman and Hall/CRC Press: Boca Raton, FL, USA, 2015.
35. Møller, J.; Syversveen, A.R.; Waagepetersen, R.P. Log Gaussian Cox Processes. *Scand. J. Stat.* **1998**, *25*, 451–482. [CrossRef]
36. Diggle, P.J.; Moraga, P.; Rowlingson, B.; Taylor, B.M. Spatial and Spatio-Temporal Log-Gaussian Cox Processes: Extending the Geostatistical Paradigm. *Stat. Sci.* **2013**, *28*, 542–563. [CrossRef]
37. Li, Y.; Brown, P.; Gesink, D.C.; Rue, H. Log Gaussian Cox processes and spatially aggregated disease incidence data. *Stat. Methods Med. Res.* **2012**, *21*, 479–507. [CrossRef] [PubMed]
38. Samartsidis, P.; Eickhoff, C.R.; Eickhoff, S.B.; Wager, T.D.; Barrett, L.F.; Atzil, S.; Johnson, T.D.; Nichols, T.E. Bayesian Log-Gaussian Cox Process Regression: Applications to Meta-Analysis of Neuroimaging Working Memory Studies. *J. R. Stat. Soc. Ser. C Appl. Stat.* **2018**, *68*, 217–234. [CrossRef]
39. Moraga, P. *Geospatial Health Data: Modeling and Visualization with R-INLA and Shiny*; Chapman & Hall/CRC Biostatistics Series; Chapman & Hall/CRC: Boca Raton, FL, USA, 2019.
40. Valente, F.; Laurini, M. A spatio-temporal analysis of fire occurrence patterns in the Brazilian Amazon. *Sci. Rep.* **2023**, *13*, 12727. [CrossRef] [PubMed]
41. Rue, H.; Held, L. *Gaussian Markov Random Fields: Theory and Applications*; CRC Press: Boca Raton, FL, USA, 2005.
42. Lindgren, F.; Rue, H.; Lindström, J. An explicit link between Gaussian fields and Gaussian Markov random fields: The stochastic partial differential equation approach. *J. R. Stat. Soc. Ser. (Stat. Methodol.)* **2011**, *73*, 423–498. [CrossRef]
43. Laurini, M.P. The spatio-temporal dynamics of ethanol/gasoline price ratio in Brazil. *Renew. Sustain. Energy Rev.* **2017**, *70*, 1–12. [CrossRef]
44. Harvey, A.C. *Forecasting, Structural Time Series Models and the Kalman Filter*; Cambridge University Press: Cambridge, UK, 1990.
45. Rue, H.; Martino, S.; Chopin, N. Approximate Bayesian inference for latent Gaussian models by using integrated nested Laplace approximations. *J. R. Stat. Soc. Ser. (Stat. Methodol.)* **2009**, *71*, 319–392. [CrossRef]

46. Hotta, L.K. Identification of Unobserved components models. *J. Time Ser. Anal.* **1989**, *10*, 259–270. [CrossRef]
47. Hardesty, J.; Myers, R.; Fulks, W. Fire, ecosystems, and people: A preliminary assessment of fire as a global conservation issue. *JSTOR* **2005**, *22*, 78–87.
48. Pivello, V.R. The use of fire in the Cerrado and Amazonian rainforests of Brazil: Past and present. *Fire Ecol.* **2011**, *7*, 24–39. [CrossRef]
49. Pivello, V.R.; Vieira, I.; Christianini, A.V.; Ribeiro, D.B.; da Silva Menezes, L.; Berlinck, C.N.; Melo, F.P.; Marengo, J.A.; Tornquist, C.G.; Tomas, W.M.; et al. Understanding Brazil's catastrophic fires: Causes, consequences and policy needed to prevent future tragedies. *Perspect. Ecol. Conserv.* **2021**, *19*, 233–255. [CrossRef]
50. Whittle, P. On stationary processes in the plane. *Biometrika* **1954**, *41*, 434–449. [CrossRef]
51. Martino, S.; Rue, H. Implementing Approximate Bayesian Inference using Integrated Nested Laplace Approximation: A Manual for the Inla Program. Technical Report. 2020. Available online: https://inla.r-inla-download.org/r-inla.org/doc/inla-manual/inla-manual.pdf (accessed on 31 January 2023).
52. Bakka, H.; Krainski, E.; Bolin, D.; Rue, H.; Lindgren, F.L. The diffusion-based extension of the Matérn field to space-time. *arXiv* **2020**, arXiv:2006.04917. Available online: https://arxiv.org/abs/2006.04917 (accessed on 31 January 2023).